J Solid State Electrochem (2006) 10: 920–928
DOI 10.1007/s10008-005-0038-2

ORIGINAL PAPER

Joan Gregori · David Gimenez-Romero
Jose Juan Garcia-Jareño · Francisco Vicente

Calculation of the rate constants of nickel electrodissolution in acid medium from EIS

Received: 7 April 2005 / Revised: 27 April 2005 / Accepted: 14 June 2005 / Published online: 2 August 2005

Abstract A kinetic analysis of the electrochemical impedance spectra for nickel electrodissolution in an acid medium based on the characteristic points of the faradaic impedance function has been performed when chloride ions are present in the acid medium. Moreover, the obtained results are compared with the event when chloride ions are not present in the acid medium. Chloride ions cause a decrease in both Γ_1 and Γ_2 surface concentration assuming a two consecutive electron transfer mechanisms, Ni(0) → Ni(I) + e^- → Ni(II) + e^-, followed by a dissolution process, Ni(II) → $Ni^{2+}{}_{aq}$. An increase of the pH favors the formation of a $Ni(OH)_2$ passive layer that impedes to distinguish clearly between both electron transfers from electrochemical impedance results.

List of Symbols

Γ_0	Steady-state surface concentration of active Ni(0)
Γ_1	Steady-state surface concentration of intermediate Ni(I)
Γ_2	Steady-state surface concentration of formed Ni(II)
k_i	Kinetic constant for each reaction step
E_0	Stabilization potential
F	Faraday constant
S	Electrode geometrical area
k_{0i}	Preexponential factor of the kinetic constant of the transfer i
b_i	Exponential factor of the kinetic constant of the electron transfer i
R_U	Uncompensated resistance
R_{ct}	Charge-transfer resistance
C_{dl}	Double-layer capacitance
C	Capacitance
R	Resistance
L	Inductance
t	Time
ω	Angular frequency
Z_F	Faradaic impedance
Z	Electrode impedance
i_M	Current intensity associated with metal electrodissolution
i	Electrode current
θ	Surface fraction covered by a passive film
$\phi_{m/f}$	Potential drop at the metal/film interface

J. Gregori · D. Gimenez-Romero · J. J. Garcia-Jareño · F. Vicente (✉)
Department of Physical Chemistry,
University of Valencia, C/Dr. Moliner 50,
46100 Burjassot, Spain
E-mail: Francisco.Vicente@uv.es

Introduction

Nickel has been the subject of many researches related with dissolution and passivation mechanisms in acid medium by means of different electrochemical techniques [1–11]. However, several points are yet unclear due to the strong tendency for self-passivation of nickel and, thus, the process of active dissolution, passive layer formation and chemical dissolution depends on a great number of variables: history of the electrodes, media, roughness of the surface, hydrodynamic conditions, metal impurities on the surface, etc [4]. A two consecutive electron transfers can be considered for early stages of nickel electrodissolution, as is frequently postulated in the electrodissolution of other similar metals in certain experimental conditions [1, 6–9, 11–17]:

$$Ni(0)(\Gamma_0) \xrightarrow{k_1} Ni(I)(\Gamma_1) + e^- \xrightarrow{k_2} Ni(II)(\Gamma_2), \quad (1)$$

$$Ni(II)(\Gamma_2) \xrightarrow{k_3} Ni^{2+}_{aq}, \quad (2)$$

where the first and the second steps are two consecutive irreversible single-electron transfers and the third one is a physical process that consists of the solubilization of Ni (II) species and the transport of a solvated Ni^{2+}

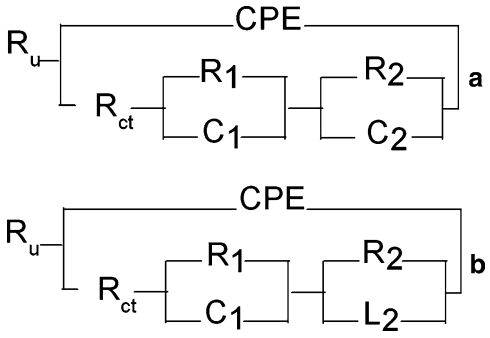

Fig. 1 Equivalent circuit used in the fitting procedure in the absence **a**, or the presence of chloride ions in the acid medium **b**. $Z_{\mathrm{CPE}} = 1/A(j\omega)^n$

throughout the aqueous media. Γ_1 and Γ_2 represent the surface concentration of Ni(I) and Ni(II) species, respectively, and rate constants of both electron transfers agree with the Butler–Volmer equation.

Following these previous works, a kinetic analysis was performed based on the fitting to the equivalent circuit of Fig. 1a or b depending on whether or not an inductive loop was defined at low frequencies. In the absence of chloride ions it was observed that $k_1 >> k_2$, k_3 and Γ_2 surface concentration increased for more anodic stabilization potentials [6].

In this work, the previous analysis has been extended to the case in which chloride ions are present in the medium, and the equations which define the characteristic points of the impedance curves in the Nyquist plot are used in order to obtain kinetic information. The results based on the analysis of the singular points and the equivalent circuit fitting procedure are compared. Also, the kinetic analysis is extended to the impedance spectra recorded at other experimental conditions in order to explain the peculiar behavior of the nickel when compared with zinc [17].

Theoretical impedance function and singular points

The theoretical faradaic impedance function, which corresponds to the reaction scheme defined by Eqs. 1 and 2, can be expressed as [6, 12, 16]:

$$FSZ_{\mathrm{F}} = \frac{k_1k_2 + (k_1 + k_2)k_3 + (k_1 + k_2 + k_3)j\omega - \omega^2}{2k_1k_3k_2b_2\Gamma_1 + 2k_2k_3k_1b_1\Gamma_0 + (k_1k_2b_2\Gamma_1 + 2k_2k_1b_1\Gamma_0 + k_3k_1b_1\Gamma_0 + k_3k_2b_2\Gamma_1)j\omega - (k_1b_1\Gamma_0 + k_2b_2\Gamma_1)\omega^2}, \quad (3)$$

where F stands for the Faraday constant, S represents the electrode geometrical area, and the other symbols have been defined in the above section. In the above equation, the values for all constant rates as well as the surface concentrations Γ_i are referred to the steady-state approximation. In the case of zinc electrodissolution, an analysis based on the characteristic points of the impedance spectra was very useful for graphically obtaining kinetic information about each elemental step in electrodissolution process [17]. For obtaining all the following equations, it is considered that $k_1 >> k_2$, k_3 [6]. In this case, the equations that define the characteristic point at which the imaginary component of the faradaic impedance shows a minimum value in the Nyquist plot can be expressed as:

$$\omega^{Z_{\mathrm{Fimag}}\mathrm{minimum}} = \frac{k_1}{1 + b_1/b_2}, \quad (4)$$

$$FSZ_{\mathrm{Fimag}}^{Z_{\mathrm{Fimag}}\mathrm{minimum}} = \frac{-b_1}{2k_1\Gamma_0b_2(b_1 + b_2)}, \quad (5)$$

$$FSZ_{\mathrm{Freal}}^{Z_{\mathrm{Fimag}}\mathrm{minimum}} = \frac{1}{2}\left(\frac{1}{k_1\Gamma_0b_2} + \frac{1}{k_1\Gamma_0(b_1 + b_2)}\right) \quad (6)$$

and for the characteristic point at which the imaginary component of the faradaic impedance shows a maximum value:

$$\omega^{Z_{\mathrm{Fimag}}\mathrm{maximum}} = 2k_3, \quad (7)$$

$$FSZ_{\mathrm{Fimag}}^{Z_{\mathrm{Fimag}}\mathrm{maximum}} = \frac{(k_3 - k_2)}{4k_3k_1\Gamma_0b_2}, \quad (8)$$

$$FSZ_{\mathrm{Freal}}^{Z_{\mathrm{Fimag}}\mathrm{maximum}} = \frac{1}{2}\left(\frac{1}{k_1\Gamma_0b_2} + \frac{k_2 + k_3}{2k_1\Gamma_0b_2k_3}\right). \quad (9)$$

It is interesting to observe that if $k_3 > k_2$, Eq. 8 implies that $Z_{\mathrm{Fimag}}^{Z_{\mathrm{Fimag}}\mathrm{maximum}}$ is positive and the maximum is defined in the fourth quadrant in the Nyquist plot, that is, an inductive loop will be observed at low frequencies. But if $k_2 > k_3$, $Z_{\mathrm{Fimag}}^{Z_{\mathrm{Fimag}}\mathrm{maximum}}$ would be negative, and consequently, a capacitive loop will be observed at low frequencies since in this case a second minimum would be defined in the first quadrant of the Nyquist plot.

Finally, the intersect point with the real axis, which is characterized by a real component of the faradaic impedance, is defined as:

$$FSZ_{\mathrm{Freal}}^{Z_{\mathrm{Fimag}}=0} = \frac{1}{k_1\Gamma_0b_2}. \quad (10)$$

The theoretical impedance function defined by Eq. 3 is equivalent to the impedance expression, which corresponds to the equivalent circuit of Fig. 1a, when a capacitive loop is defined at low frequencies, or to the impedance expression of the equivalent circuit of Fig. 1b, when an inductive loop is observed at low frequencies [18, 19]. Nevertheless, it should be noticed that there are several different circuit models that behave as a capacitive or inductive loop [14, 20]. In both cases the equations which relate the kinetic parameters with the passive elements of the equivalent circuits are:

$$\frac{k_2 + k_3}{2k_1k_3b_2\Gamma_0} = F(R + R_1 + R_2), \tag{11}$$

$$\frac{1}{2k_1k_3b_2\Gamma_0} = F(R(R_1C_1 + R_2C_2) + R_1R_2(C_1 + C_2)), \tag{12}$$

$$\frac{1}{2k_3} = R_1C_1 + R_2C_2, \tag{13}$$

$$\frac{b_1 + b_2}{2k_1k_3b_2} = R_1R_2C_1C_2 \tag{14}$$

and:

$$\frac{k_2 + k_3}{2k_1k_3b_2\Gamma_0} = F(R + R_1)_1, \tag{15}$$

$$\frac{1}{2k_1k_3b_2\Gamma_0} F\frac{(L_2(R + R_1 + R_2) + RR_1R_2C_1)}{R_2}, \tag{16}$$

$$\frac{1}{2k_3} = \frac{R_2R_1C_1 + L_2}{R_2}, \tag{17}$$

$$\frac{b_1 + b_2}{2k_1k_3b_2} = \frac{R_1C_1L_2}{R_2}, \tag{18}$$

respectively.

Experimental section

All the experiments have been carried out in a typical three electrodes cell. The potential was measured with Ag/AgCl/KCl (sat.) reference electrode such that all the potentials in this work have been referred. A platinum sheet of a relatively large area ($S = 2$ cm^2) was used as an auxiliary electrode. Solutions were prepared from K_2SO_4 (Probus, a.g.), H_2SO_4 (Merk, a.g.), KCl (Fluka, a.g.), Na_2SO_4 (Sigma, a.g.), H_3BO_3 (R.P. Normapur, a.g.) and NH_4Cl (Panreac, a.g.),with distilled and double deionized water (MilliQ).

For impedance measurements, the potential was controlled by a Potentiostat-Galvanostat 273A EG&G PAR and the impedance spectra was recorded with the help of a Lock-in Amplifier 5210 EG&G PAR. The working electrodes were made from a nickel sheet (99.9%, Johnson&Matthey). The stabilization potential E_0 was applied for 60 min before recording the impedance spectrum. The impedance measurements were carried out in the frequency range [10^5, 5×10^{-2}] Hz and the amplitude of the harmonic potential perturbation was 5 mV rms. All the measurements were carried out at constant and controlled temperature $T = 297.8 \pm 0.1$ K. All solutions were deaerated by bubbling Ar (Air Liquide) for 5 min before starting the experiment. All the impedance measurements have been performed under inert atmosphere and still conditions. The fitting of the experimental impedance data to the proposed equivalent circuit was carried out by means of a non-linear least squares procedure based on the Marquardt algorithm for function optimization [21, 22]. All the errors determined from multi-parametrical fitting are less than 10%. The faradaic impedance Z_F is obtained from the measured electrode impedance Z according to the equation:

$$\frac{1}{Z_F} = \frac{1}{Z - R_U} - j\omega C_{dl}, \tag{19}$$

where R_U represents the uncompensated resistance associated with the electrolyte and the electrode contacts, and C_{dl} stands for the double-layer capacitance.

Results and discussion

Nickel electrodissolution

Figure 2 shows the experimental impedance spectra for a nickel polycrystalline electrode recorded in an acid medium which contains 0.1 M KCl.

In this case, at intermediate frequencies the characteristic point at which the imaginary component of the faradaic impedance shows a min imum value is well defined, as well as the characteristic point at which the imaginary component of the faradaic impedance shows a maximum at low frequencies. Table 1 shows the impedance values which define these characteristic points as a function of the stabilization potential.

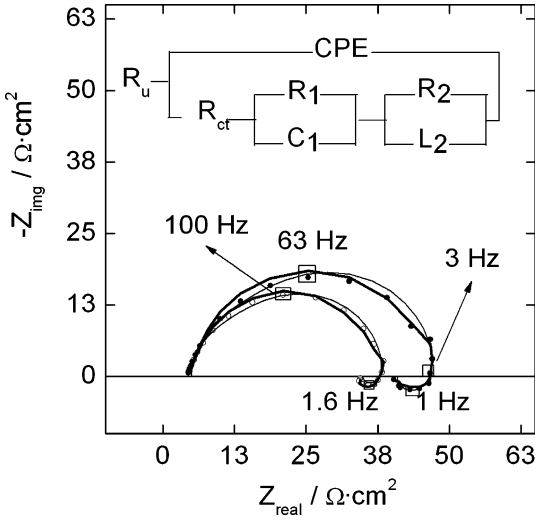

Fig. 2 Experimental impedance spectra (*symbol*), simulated (*solid line*) and fitting to the equivalent circuit of Fig. 1b (*bold line*), at the stabilization potentials $E_0 = -110$ mV (*full circles*) and $E_0 = -100$ mV (*open circles*). 0.245 M K_2SO_4, 5×10^{-3} M H_2SO_4, 0.1 M KCl. pH = 2.7. T = 298 K. Simulations of the impedance spectra have been made with the following parameters: $E_0 = -110$ mV, $k_1 = 698$ s^{-1}, $k_2 = 3.8$ s^{-1}, $k_3 = 5$ s^{-1}, $\Gamma_1 = 1\times10^{-9}$ mol cm^{-2}, $b_1 = 38$ V^{-1}, $b_2 = 50$ V^{-1}; $E_0 = -110$ mV, $k_1 = 1105$ s^{-1}, $k_2 = 6.3$ s^{-1}, $k_3 = 8$ s^{-1}, $\Gamma_1 = 0.9\times10^{-9}$ mol cm^{-2}, $b_1 = 38$ V^{-1}, $b_2 = 50$ V^{-1}

Table 1 Evolution with respect to the stabilization potential E_0 of characteristic points of the impedance function of the nickel anodic dissolution

E (V)	ω_{min} (s^{-1})	Z_{Fim}^{min} (Ω cm^2)	Z_{Freal}^{min} (Ω cm^2)	ω_{max} (s^{-1})	Z_{Fim}^{max} (Ω cm^2)	Z_{Freal}^{max} (Ω cm^2)	$Z_{Freal}^{Z_{Fim}=0}$ (Ω cm^2)
−0.135	157	−40	123	2.3	10	164	171
−0.125	251	−15	81	6.3	7	82	88
−0.110	396	−8	34	10	3	40	43
−0.100	628	−6	28	16	2	32	34

The experimental conditions are the same as in Fig. 2

As can be seen in Table 1, as the measured intensity current increases, there is a shift of the characteristic frequencies towards higher values, as well as the imaginary and real components of the impedance decrease. The equation system defined by Eqs. 4, 7, 8 and 10 allows to obtain the kinetic parameters for nickel electrodissolution in these experimental conditions as a first approach. For this purpose a previously described iterative procedure is used [16]: first, initial values for b_1 and b_2 are supposed. Then, k_1, k_2, k_3 and Γ_0 values are calculated from the above-considered equation system. It is considered that k_1 and k_2 follow a Butler–Volmer relationship with the applied potential E_0:

$$k_i = k_{0i} e^{b_i E_0} \tag{20}$$

and from the slope of the ln k_i versus E_0 plot, b_i values are recalculated. In this way, an iterative procedure is performed until a convergence for b_i is found. Moreover, from the steady-state approximation:

$$k_1\Gamma_0 = k_2\Gamma_1 = k_3\Gamma_2 \tag{21}$$

which allows, once k_1, k_2, k_3 and Γ_0 values are known, to calculate Γ_1 and Γ_2 values.

Table 2 shows the obtained values for k_1, k_2, k_3, Γ_1 and Γ_2 as a function of the stabilization potential.

In this case, Γ_1 and Γ_2 values show a parallel evolution; these values increase until a maximum is reached and then decrease. Moreover, Γ_1 values are higher than Γ_2 values in all the explored potential range. Also, it is observed that k_3 values are higher than k_2 values. According to Eq. 8 this fact implies that an inductive loop would be defined at low frequencies as is experimentally observed.

k_1 and k_2 values are compared with those obtained from the equivalent circuit analysis. For this purpose, equation system 15, 16, 17 and 18 is used and the equivalent circuit used in the fitting procedure is that of Fig. 1b. Table 3 shows the values for the passive elements of the equivalent circuit which result from the fitting procedure.

The obtained values for k_1 and k_2 are represented in Fig. 3 in the form of lnk_i versus E_0 plots, where E_0 represents the stabilization electrode potential. There is a good agreement between the values obtained with both analysis methods, and also for the values obtained for b_1 and b_2 parameters. Finally, from the obtained kinetic parameters values, the impedance spectra have been

Table 2 Kinetic parameters, k_i, and surface concentration of Ni(I) species, Γ_1, and Ni(II) species, Γ_2, on the electrode surface as a function of the applied potential

E(V)	i (μA cm^{-2})	k_1 (s^{-1})	k_2 (s^{-1})	k_3 (s^{-1})	Γ_1 (mol cm^{-2})	Γ_2 (mol cm^{-2})
−0.135	204	276	1.2	1.5	8.8×10^{-10}	7.0×10^{-10}
−0.125	354	441	2.0	3.2	9.2×10^{-10}	5.8×10^{-10}
−0.110	890	696	3.8	5.0	12×10^{-10}	9.2×10^{-10}
−0.100	1142	1105	6.3	8.0	9.4×10^{-10}	8.4×10^{-10}

The experimental conditions are the same as in Fig. 2

Table 3 Determined values of the passive element of the equivalent circuit which result from the fitting procedure. The impedance of CPE is noted as $Z_{CPE} = 1/A(j\omega)^n$. In all cases $R_U = 6$ Ω cm^2

E(V)	n	A (F cm^{-2} s^n)	R_{ct} (Ω cm^2)	R_1 (Ω cm^2)	C_1 (F cm^{-2})	R_2 (Ω cm^2)	L_2 (H cm^{-2})
−0.135	0.95	4.0×10^{-5}	100	45	2.2×10^{-4}	23	10
−0.125	0.95	2.8×10^{-5}	58	15	1.9×10^{-4}	13	2
−0.110	0.95	4.4×10^{-5}	23	14	1.6×10^{-4}	6	0.5
−0.100	0.95	3.6×10^{-5}	18	11	1.2×10^{-4}	5	0.4

The experimental conditions are the same as in Fig. 2

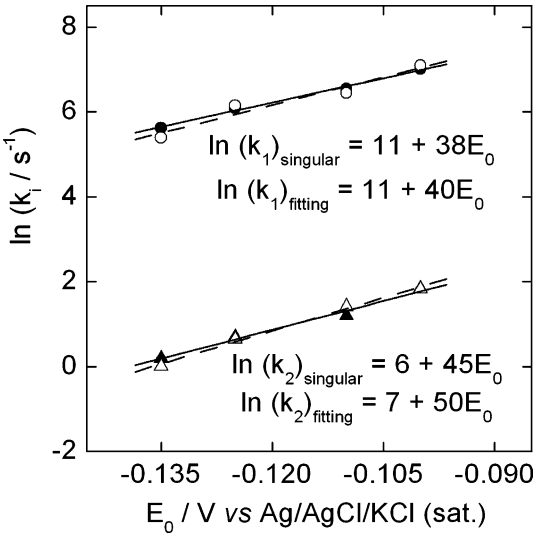

Fig. 3 Comparison of kinetic constants' values k_1 and k_2 obtained with singular points analysis (*full symbols*) and equivalent circuit analysis (*open symbols*)

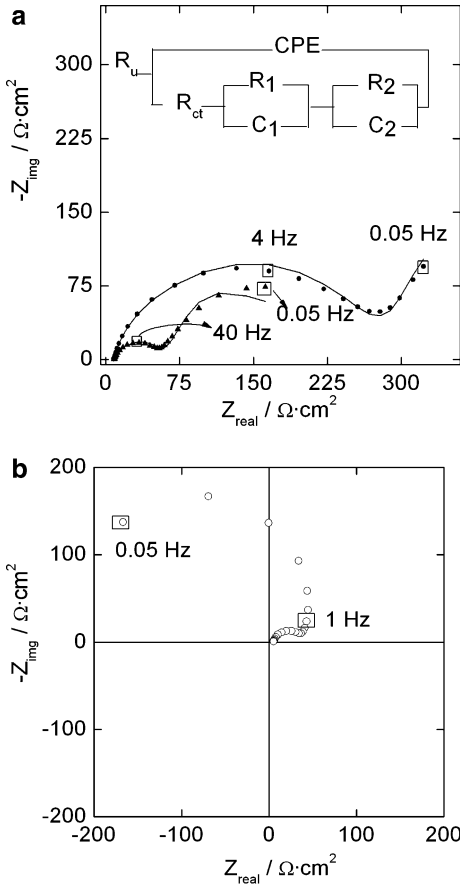

Fig. 4 **a** Experimental impedance spectra at $E_0 = -125$ mV (*full circles*) and $E_0 = -50$ mV (*full up triangles*). 0.245 M K_2SO_4, 5×10^{-3} M H_2SO_4. pH = 2.7. $T = 298$ K. *Solid line* indicates the fitting to the equivalent circuit of Fig. 1a. **b** Experimental impedance spectra at $E_0 = -0$ mV, $i_0 = 1862$ μA cm^{-2}. Experimental conditions are the same as in previous case

simulated, and, as can be seen in Fig. 1, there is a good agreement between experimental and simulated curves, and also for the potential evolution of the measured spectra.

Then, in these experimental conditions, nickel electrodissolution can be described by means of the proposed mechanism through reactions 1 and 2.

Active/passive transition

Figure 4a shows the experimental impedance spectra for a nickel polycrystalline electrode recorded at two different stabilization potentials in the [−125,−25] mV potential range at the same acid medium in the absence of chloride ions.

As can be seen in Fig. 4a, in this case, the characteristic point at low frequencies is not well defined. Subsequently, the impedance spectra have been fitted to the equivalent circuit of Fig. 1a, in order to obtain kinetic information about electrodissolution process. In that case, the experimental uncertainty is greater than the one associated at the mathematical calculation of the magnitudes. All the errors determined from multiparametrical fitting are less than 10%. Moreover, the used fitting program automatically detects the parameter indetermination [21, 22]. Table 4 shows the values for the passive elements of the equivalent circuit which result from the fitting procedure in this case.

As can be seen in Fig. 4a, there is a good agreement between experimental and fitted impedance spectra.. The solution of the equation system defined by Eqs. 11, 12, 13 and 14 allow to obtain numerical values for k_1, k_2, k_3,

Table 4 Determined values of the passive element of the equivalent circuit which result from the fitting procedure. The impedance of CPE is noted as $Z_{CPE} = A(j\omega)^n$. In all cases $R_U = 6$ Ω cm^2

E(V)	n	A (F cm^{-2} s^n)	R_{ct} (Ω cm^2)	R_1 (Ω cm^2)	C_1 (F cm^{-2})	R_2 (Ω cm^2)	C_2 (F cm^{-2})
−0.125	0.85	1.6×10^{-4}	215	60	9.8×10^{-4}	275	28×10^{-3}
−0.100	0.85	1.9×10^{-4}	150	45	8.7×10^{-4}	260	20×10^{-3}
−0.075	0.85	2.1×10^{-4}	75	30	6.1×10^{-4}	240	15×10^{-3}
−0.050	0.85	1.5×10^{-4}	35	15	5.9×10^{-4}	125	127×10^{-3}
−0.025	0.85	1.0×10^{-4}	20	10	6.5×10^{-4}	100	12×10^{-3}

The experimental conditions are the same as in Fig. 4

Table 5 Kinetic parameters, k_i, and surface concentration of Ni(I) species, Γ_1, and Ni(II) species, Γ_2, on the electrode surface as a function of the applied potential

E (V)	i(μA cm^{-2})	k_1 (s^{-1})	k_2 (s^{-1})	k_3 (s^{-1})	Γ_1 (mol cm^{-2})	Γ_2 (mol cm^{-2})
−0.125	191	27	0.2	0.1	5.0×10^{-9}	1.0×10^{-8}
−0.100	274	45	0.4	0.1	3.7×10^{-9}	1.5×10^{-8}
−0.075	533	94	0.8	0.2	3.5×10^{-9}	1.5×10^{-8}
−0.050	1130	168	1.8	0.3	3.3×10^{-9}	2.0×10^{-8}
−0.025	2172	277	3.4	0.5	3.2×10^{-9}	2.2×10^{-8}

The experimental conditions are the same as in Fig. 4

Γ_1 and Γ_2 parameters. For this purpose [6], Eq. 13 allows directly to calculate k_3 value. Then from Eq. 14, k_1 values are obtained, and from Eq. 12 Γ_0 values are calculated. Finally, from Eq. 11, k_2 values are determined. Then, an unique analytical solution is obtained for the kinetic parameters. Equation 21, which implies that the steady state is reached, allows to obtain Γ_1 and Γ_2 values. These values are represented in Table 5 as a function of the stabilization potential. In this case, k_2 values are higher than k_3 values, and in accordance with Eq. 8, a capacitive loop is defined at low frequencies. Also, it is observed that Γ_1 values decrease, whereas Γ_2 values increase with the stabilization potential, and these values are higher than those obtained in the presence of chloride ions in the acid medium.

Figure 4b shows the impedance spectrum recorded at the stabilization potential $E_0 = 0$ mV. At low frequencies, it shows a negative time constant that is characteristic for a passivation process which is produced at the descending part of the polarization curve. In order to analyze the active-to-passive transition, a simplified reaction mechanism is considered according to:

$$\mathrm{Ni(0)} \rightarrow \mathrm{Ni(II)} + 2\mathrm{e}^-, \tag{22}$$

$$\mathrm{Ni(II)} \rightarrow \mathrm{Ni}_{\mathrm{aq}}^{2+} \tag{23}$$

and it is considered that the covered fraction of the electrode surface by passivating species, θ, is proportional to the surface concentration of Ni(II) species at the electrode surface, Γ_2, [23–25]:

$$\theta = K\Gamma_2, \tag{24}$$

where the proportionality constant K has dimensions of cm^2 ·mol^{-1}. Thus, it is considered that the electrode surface is partially covered by a passive layer which covers a surface fraction θ due to the formation of $Ni(OH)_2$ on surface. It is also considered that K value is potential independent. Then, the measured intensity current is [25]:

$$i = i_{\mathrm{M}}(1-\theta), \tag{25}$$

where i_{M} would be the intensity value in the absence of passive layer on the electrode surface, and 1-θ is the no covered fraction of the electrode surface. If a small sinusoidal perturbation of potential of amplitude Δ E is applied around a defined steady state at a potential E_0, then the intensity variation would be:

$$\Delta i = \Delta i_{\mathrm{M}}(1-\theta) - i_{\mathrm{M}}\Delta\theta \tag{26}$$

and the admittance would be:

$$Y = \frac{1}{Z} = \frac{1}{Z_{\mathrm{F}}}(1-\theta) - i_{\mathrm{M}}\frac{\Delta\theta}{\Delta E} = \frac{1}{Z_{\mathrm{F}}}(1-\theta) - i_{\mathrm{M}}K\frac{\Delta\theta_2}{\Delta E}, \tag{27}$$

where, in this case:

$$2FSZ_{\mathrm{F}} = 2FS\frac{\Delta E}{\Delta i_{\mathrm{M}}} = \frac{1}{b_1k_1\Gamma_0} + \frac{k_1}{b_1k_1\Gamma_0}\frac{1}{k_3+j\omega}, \tag{28}$$

$$\frac{\Delta\theta_2}{\Delta E} = \frac{k_1b_1\Gamma_0}{k_1+k_3+j\omega}. \tag{29}$$

By substituting Eqs. 28 and 29 into Eq. 27, the following is obtained:

$$2FSZ = \frac{1}{(1-\theta)k_1b_1\Gamma_0} + \frac{\left(k_1+\frac{Kk_1\Gamma_0}{(1-\theta)}\right)/(k_1b_1\Gamma_0(1-\theta))}{\frac{k_3(1-2\theta)}{1-\theta}+j\omega}, \tag{30}$$

It can be demonstrated that the frequency at which Z_{Fimg} has a minimum value is defined as follows:

$$\omega^{Z_{\mathrm{Fimag}}\mathrm{minimum}} = \frac{k_3(1-2\theta)}{1-\theta}. \tag{31}$$

Equation 31 implies that a negative time constant would be observed on the impedance diagram when $\theta > 0.5$, that is, when more than one half of the electrode surface is covered by passivating species. This time constant is defined by the minimum of the imaginary component of the faradaic impedance at low frequencies. For the case of the impedance spectrum of Fig. 4b, an estimation of θ value can be made since $\omega^{Z_{\mathrm{Fimag}}\mathrm{minimum}} = 0.63\,\mathrm{s}^{-1}$. If it is considered that $k_3 = 0.5\ \mathrm{s}^{-1}$, then a value of $\theta = 0.69$ is obtained which implies that 69% of the electrode surface is covered by a passive layer.

Effect of pH on the active/passive transition

Figure 5a shows the descending part of the polarization curve for a polycrystalline nickel electrode in a weakly

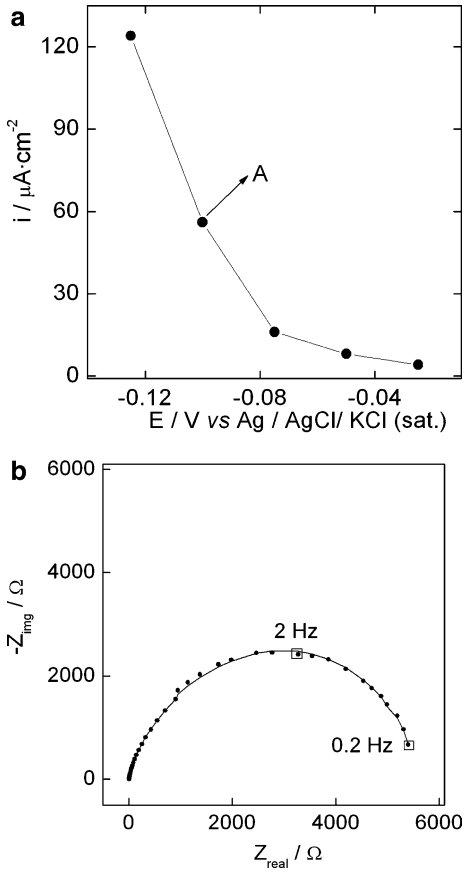

Fig. 5 **a** Steady-state current values at different stabilization potentials. 0.32 M H_3BO_3, 0.26 M NH_4Cl, 1.33 M Na_2SO_4. pH = 5.1. $T = 298$ K. **b** Experimental impedance spectra recorded at point A in the above polarization *curve*. Experimental conditions are the same as in previous case

acid medium of pH = 5.1. Figure 5b shows the impedance spectrum recorded at point A in the polarization curve. This impedance shape is the same for all the measured impedance spectra in the descending part of the polarization curve.

It is observed that the low-frequency limit of the impedance increases as the stabilization potential becomes more anodic, but in this case no negative time constant is observed in any case in the frequency range explored. This experimental finding can be explained if it is considered that a 3-D film covers the electrode surface in the active-to-passive potential range, and the intensity current is determined by the potential drop at the metal/film interface, $\phi_{m/f}$, [26]. In this way, if $\phi_{m/f}$ decreases when the stabilization potential E_0 increases, then i_F values must decrease and negative time constant would not be defined in the impedance spectra. This decrease in $\phi_{m/f}$ with the stabilization potential is determined by the passive-layer thickness and the electric field within the passive layer [27, 28]. Thus, it can be concluded that at a less acid medium (i.e. pH ≈ 5), nickel is readily covered by a 3-D film which covers the electrode surface and passivates it.

Discussion of the kinetic model based on two consecutive electron transfers

The presence of a 3-D passive layer impedes to distinguish between both single-electron transfers by means of EIS. Other different situation is reached when the Ni electrodissolution is produced at lesser pH and at lesser stabilization potentials, as it is previously commented. In this case, it is possible to distinguish between two different situations: when a 2-D passive layer is produced, Sect. 4.2, or in an ideal case in which the formation of passivated Ni-sites on electrode do not influence the electrochemical mechanism, Sect. 4.1, as occurs in the case of Zn in free oxygen solutions [17].

When chloride ions are present in the acid medium, electrochemical impedance spectra, which correspond to nickel electrodissolution, shows an inductive behavior at low frequencies, as can be seen in Fig. 2. This experimental fact supports the assumption that the nickel electrodissolution follows the general mechanism in which the chloride stabilizes the intermediate Ni(I) on the electrode surface, whereas in the case of absence of chloride in the solution, a capacitive loop can be seen in the recorded spectra, as can be seen in Fig. 4. This fact is schematized in Fig. 6, where the faradaic component of the electrode impedance is represented for both cases. From the general mechanism proposed through reactions 1and 2, this experimental behavior is determined by the relation between k_2 and k_3 kinetic constants. $k_2 < k_3$ implies an inductive behavior, whereas $k_2 > k_3$ implies a capacitive one, as it is previously indicated [6, 16].

As mentioned above, the faradaic impedance defines some characteristic points which allow the calculation of the kinetic parameters associated with the considered

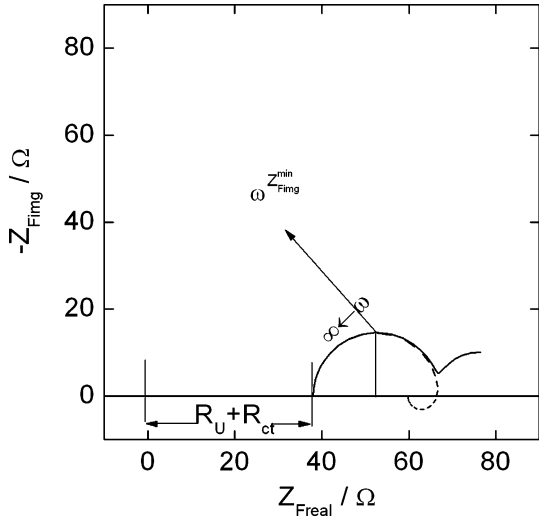

Fig. 6 Simulated impedance spectra in absence (*solid line*) and presence (*dashed line*) of 0.1 M KCl in the acid medium. $k_1 = 1105\ s^{-1}$, $k_2 = 6.3\ s^{-1}$, $\Gamma_1 = 5\times10^{-10}$ mol cm^{-2}. *Dashed line*: $k_3 = 8\ s^{-1}$, $b_1 = 38\ V^{-1}$, $b_2 = 50\ V^{-1}$; *solid line* $k_3 = 5\ s^{-1}$, $b_1 = 20\ V^{-1}$, $b_2 = 30\ V^{-1}$. 0.245 M K_2SO_4, 5×10^{-3} M H_2SO_4. pH = 2.7. $T = 298$ K

Table 6 Evolution with respect to the stabilization potential E_0 of characteristic points of the impedance function of the nickel anodic dissolution

E (V)	R_{ct} (Ω cm^2)	$k_1\Gamma_0$ (mol cm^{-2} s^{-1})
−0.135	100	1.2×10^{-9}
−0.125	60	2.0×10^{-9}
−0.110	28	4.3×10^{-9}
−0.100	19	6.2×10^{-9}

0.245 M K_2SO_4, 5×10^{-3} M H_2SO_4, 0.1 M KCl. pH = 2.7. T = 298 K

Table 7 Evolution with respect to the stabilization potential E_0 of characteristic points of the impedance function of the nickel anodic dissolution

E (V)	$\omega^{Z_{Fimag}}$ minimum (s^{-1})	R_{ct} (Ω cm^2)	$k_1\Gamma_0$ (mol cm^{-2} s^{-1})
−0.125	19	250	1.0×10^{-9}
−0.100	25	176	1.2×10^{-9}
−0.075	63	95	2.3×10^{-9}
−0.050	101	45	4.7×10^{-9}
−0.025	157	19	1.1×10^{-8}

0.245 M K_2SO_4, 5×10^{-3} M H_2SO_4. pH = 2.7. T = 298 K

electrodissolution mechanism. However, it is experimentally observed that when chloride ion is not present in the acid medium, the low-frequency capacitive loop is not well defined and consequently, nor the characteristic points of this zone of frequencies, as can be seen in Fig. 6. But the high frequency characteristic point is quite well defined in both cases. The frequency at which the imaginary component of the faradaic impedance shows a minimum is defined by Eq. 4. Moreover [13, 16]

$$\lim_{\omega\to\infty} Z_F^{Z_{Fimg}=0} = R_{ct} = \frac{1}{FSk_1\Gamma_0(b_1+b_2)}, \tag{32}$$

where S represents the electrode geometrical area and F stands for the Faraday constant. Tables 6 and 7show the graphically determined R_{ct} values as a function of the stabilization potential.

Moreover, in Tables 6 and 7, the $k_1\Gamma_0$ values calculated from equation (30) are represented. These values are a measurement of the rate of each reaction step, and, as can be seen in Tables 6 and 7, the presence of chloride ions in the acid medium enhances nickel electrodissolution causing a considerable increase in the reaction steps rate. At the steady state, the faradaic current is defined by:

$$i_F = 2FSk_1\Gamma_0. \tag{33}$$

Calculated and measured faradaic currents are compared in Fig. 7. There is a good agreement between both values.

In both cases (in absence and presence of chloride) the plot of the rate constants, calculated by fitting at low pH values (pH $\leq$ 3) versus the applied potential shows a linear dependence in accordance with a Butler–Volmer equation. This fact allows to obtain the b_i parameters of

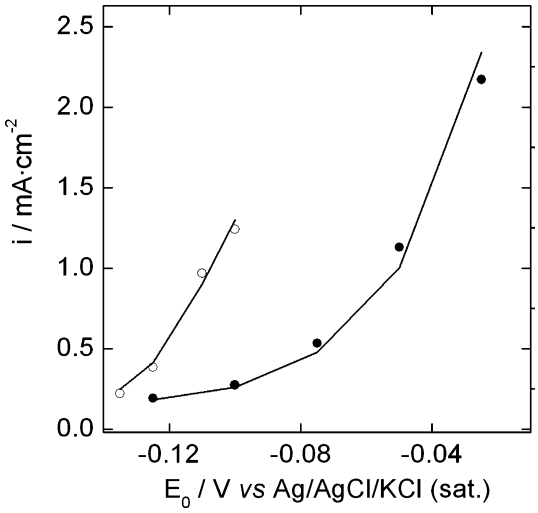

Fig. 7 Measured (*symbol*) and calculated (*solid line*) steady-state faradaic current values as a function of the stabilization potential. *Full symbols*: 0.245 M K_2SO_4, 5×10^{-3} M H_2SO_4. pH = 2.7. T = 298 K. *Open symbols*: 0.245 M K_2SO_4, 5×10^{-3} M H_2SO_4, 0.1 M KCl. pH = 2.7. T = 298 K

each single-electron transfer and, consequently, the respective electronic transfer coefficient α_i by means of the equation:

$$b_i = \frac{n_i\alpha_i F}{RT}, \tag{34}$$

where, in this case, $n_i = 1$.

For an irreversible electrochemical process which involves an overall n number of electrons, the experimental $n\alpha$ parameter, measured from the dependence of the faradaic current on the applied potential, could be related with the symmetry parameter β of each electron-transfer step by means of the following equation [29, 30]:

$$n\alpha = v[(j-1)+\beta+\omega'], \tag{35}$$

where j is the number of rate-determining step and ω' includes the environmental effect on the rate determining electron transfer j. Obviously, in the case of Ni oxidation, $n = 2$, the number of electrons transferred in the rate-determining step could be $v = 1$ or $v = 2$ depending on the single-electron transfers occurring separately or simultaneously, respectively. Different possibilities are discussed in Table 8, where the obtained values for the parameters which appear in Eq. 35 are represented for nickel electrodissolution in the presence and absence of chloride, respectively.

Due to the fact that the hydroxyl ions have negative charge, the situation of $v = 2$ and $j = 1$ is the most probable possibility for an adiabatic electron transference in the case where chloride ions are not present in the acid medium. Then, in this case, it is not possible to distinguish the determining single-electron transfer by EIS, and consequently, the calculated kinetic parameters of both consecutive steps by means of the fitting to the Eq. 3 is a very simple approximation to the reality.

Table 8 Semilogarithmic dependence of k_i and i_F on the potential

$\ln k_i = a_i + b_i E$; $\ln i_F = a + bE$	a_1	b_1 (V^{-1})	a_2	b_2 (V^{-1})	a	b (V^{-1})	$n\alpha$	β	v	j	w'
Acid medium with chloride[a]	9	28	6	45	−2	51	1.31	0.5	1	2	−0.19
Acid medium without chloride[b]	6	23	2	28	−2	26	0.68	0.5	1	2	−0.82
									1	1	0.16
									2	1	−0.16

It is assumed a symmetry factor $\beta = 0.5$ in the calculations for each single electron transfer. I_F values have been measured under potentiostatic conditions after 1 h of polarization at each applied potential [a] 0.245 M K_2SO_4, 5×10^{-3} M H_2SO_4, 0.1 M KCl. pH = 2.7 [b] 0.245 M K_2SO_4, 5×10^{-3} M H_2SO_4. pH = 2.7

From a formal point of view, the experimental $n\alpha$ experimental values seems also to be explained by means of $j = 1$ and $v = 1$ or $j = 2$ and $v = 1$, from the semilogarithmic plots. However, these two possibilities are less probable due to the sign and magnitude of the calculated ω' parameters and, independently of these consideration, the calculated b_i values by EIS give evidence that both single-electron transfers are similarly activated by the change of the stabilization potential. But, when chloride stabilizes the Ni(I) intermediate, it seems that the general model proposed by the dissolution is valid since neither 2-D nor 3-D passive layers hinder the faradaic process across two consecutive single-electron transfers where $j = 2$ and $v = 1$.

Conclusions

Nickel electrodissolution takes place according to two mono-electron transfers followed by a transport step through a layer formed by Ni(I) and Ni(II) species which most probably has a gel-like structure consistent with visual naked eye observations. An analysis based on the singular points of the faradaic impedance function shows that when the acid medium contains chloride ions, this layer is diminished with respect to the surface concentrations of Ni(I) and Ni(II). This analysis is consistent with that based on the fitting to an equivalent circuit with two time constants, which has been already used when chloride ion is not present. Thus, it seems that the active-to-passive transition consists on a progressive transformation of the above non-passivating layer to a more passivating one as the stabilization potential becomes more anodic. However, at a less acid medium, it seems that a three-dimensional layer already covers the whole electrode surface at the active/passive potential range.

Acknowledgements This work has been supported by CTQ 2004-08026/BQU. J. Gregori acknowledges a Fellowship from the Spanish Education Ministry (FPU program). J.J. García-Jareño acknowledges their position (Program "Ramón y Cajal") to the Spanish Education and Science Ministry.

References

1. Sato N, Okamoto G (1964) J Electrochem Soc 111:897
2. Bockris JO'M, Reddy AKN, Rao B (1966) J Electrochem Soc 113:1133
3. Real SG, Vilche JR, Arvía AJ (1980) Corros Sci 20:563
4. Barbosa MR, Real SG, Vilche JR, Arvía AJ (1988) J Electrochem Soc 135:1077
5. MacDougall B (1979) J Electrochem Soc 126:919
6. Gregori J, García-Jareño JJ, Giménez D, Vicente F (2005) J Solid State Electrochem 9:83
7. Jouanneau A, Keddam M, Petit MC (1976) Electrochim Acta 21:287
8. Barbosa MR, Bastos JA, Gacía-Jareño JJ, Vicente F (1998) Electrochim Acta 44:957
9. Keddam M, Takenouti H, Yu N (1985) J Electrochem Soc 132:2561
10. Keddam M (1995) Corrosion Mechanism in theory and practice. In: Marcus P, Oudar J (eds) Marcell Dekker, New York, pp 55–122
11. Itagaki M, Nakazawa H, Watanabe K, Noda K (1997) Corros Sci 39:901
12. Giménez-Romero D, García-Jareño JJ, Vicente F (2003) J Electroanal Chem 558:25
13. Giménez-Romero D, García-Jareño JJ, Vicente F (2003) Electrochem Commun 5:722
14. Shao HB, Wang JM, Zhang Z, Zhang JQ, Cao CN (2003) J Electroanal Chem 549:145
15. García-Jareño JJ, Giménez-Romero D, Vicente F (2004) Appl Surf Sci 238:449
16. García-Jareño JJ, Giménez-Romero D, Keddam M, Vicente F (2005) J Phys Chem B 109:4584
17. García-Jareño JJ, Giménez-Romero D, Keddam M, Vicente F (2005) J Phys Chem B 109:4593
18. Giménez-Romero D, García-Jareño JJ, Vicente F (2004) J Electroanal Chem 572:235
19. Cai M, Park S-M (1996) J Electrochem Soc 143:3895
20. Wu XJ, Ma HY, Chen SH, Xu Zy, Sui AF (1999) J Electrochem Soc 146:1847
21. Macdonald JR (1992) Solid State Ionics 58:97
22. Vicente F, García-Jareño JJ, Sanmatías A (2000) Procesos Electródicos del NAFIÓN y del Azul de Prusia sobre electrodo transparente de óxido de indio-estaño: un modelo de electrodo multicapa. Moliner-40, Burjassot
23. Cachet C, Saidani B, Wiart R, (1992) J Electrochem Soc 139:644
24. Chenebault P, Vallin D, Thevenin J, Wiart R(1989) J Appl Electrochem 19: 413
25. EbersbacU, Schwabe K, Ritter K(1967) Electrochim Acta 12:927
26. D'Alkaine CV, Santanna MA (1998) J Electroanal Chem 457:13
27. 27. Olsson COA, Hamm D, Landolt D (2000) J Electrochem Soc 147:4093
28. Macdonald DD, Biaggio SR, Song H (1992) J Electrochem Soc 139:170
29. Devanathan MA (1972) Electrochim Acta 17:1683
30. Nuñez_Flores MA, Ruano A, Vicente F (1988) Anales de Química 84:289